Lithium Batteries

DOI: 10.1002/ange.200906287

A Critical Size of Silicon Nano-Anodes for Lithium Rechargeable Batteries**

*Hyejung Kim, Minho Seo, Mi-Hee Park, and Jaephil Cho**

Due to the high theoretical capacity (ca. 4200 mAh g^{-1}) of Si when $Li_{4.4}Si$ is formed, it has been extensively investigated for use as a high-capacity anode material that can replace graphite, which is currently used (372 mAh g^{-1}). However, Si exhibits significant volume changes (> 360 %) during Li alloying and dealloying. These changes cause cracking and crumbling of the electrode material and a consequent loss of electrical contact between individual particles and hence severe capacity drop.[1] However, such mechanical strain induced by volume change can be reduced by employing smaller particles.[2–4] To this end, synthetic methods such as spark ablation,[5] aerogel techniques,[6,7] and sputtering[8,9] have been employed. Formation of crystalline Si nanoparticles requires higher temperatures due to the more covalent nature of these particles compared to Ge particles, and at low temperature amorphous phases become more common.

The first commonly recognized successful production of Si nanoclusters was reported by Heath et al.[10] They showed that Si nanocrystals capped with alkyl groups can be produced by reduction of $SiCl_4$ and $RSiCl_3$ ($R = H, C_8H_{17}$) according to the reaction[10] $SiCl_4 + RSiCl_3 + Na \rightarrow Si + NaCl$. This process was carried out at high temperature (385 °C) and high pressure (>100 atm) in a steel bomb fitted into a heating mantle. A process that utilizes $SiCl_4$ reduction at room temperature under an inert atmosphere was initially reported by Kauzlarich et al.[11] However, the drawback of their method was that the product obtained at room temperature was not fully crystallized and was severely capped with alkyl terminators. Moreover, an annealing process above 900 °C is required to obtain the crystalline phase.[12] Similar solution syntheses have been reported at low or high temperature after reducing Si salts with $LiAlH_4$[13,14] or alkyl silanes.[15] However, all of these methods produce a broad particle size distribution or involve aggregation of the nanoparticles. Furthermore, they all yield amounts of material too small for use in anode production for lithium secondary batteries.

We now report a synthetic method using reverse micelles at high pressure and temperature in a bomb that produces Si nanoparticles (n-Si) with various particle sizes without aggregation and thus enables the optimal nanoparticle size for use in anode materials to be chosen.

Figure 1 shows the XRD pattern and TEM images of n-Si prepared with trimethyloctadecylammonium bromide (OTAB) surfactant. The XRD pattern clearly shows formation of a diamond cubic phase. The particle size, as estimated by the Scherrer formula, was (5 ± 0.4) nm. The high-resolution TEM image (Figure 1c) shows the lattice fringes of the (311) plane corresponding to the *d* spacing of 1.6 Å of Si phase. X-ray photoelectron spectroscopy (XPS) of the 5 nm sized n-Si (Figure 1d) revealed a strong peak at about 100 eV, which indicates the presence of metallic Si. In the case of SiO_2, two dominant peaks at 110 and 105 eV are observed; therefore, the shoulders at about 104 eV for the n-Si sample are indicative of the formation of SiO_x with $x < 2$.[18]

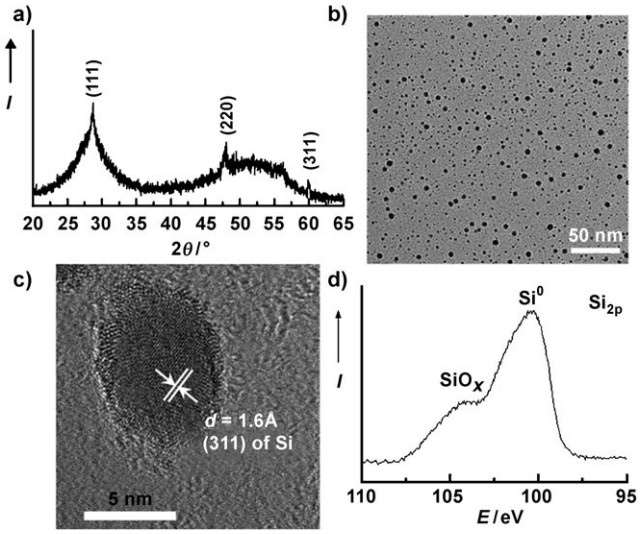

Figure 1. a) XRD pattern, b) and c) TEM images, and d) XPS spectrum of the 5 nm sized n-Si prepared with OTAB surfactant (*I*: intensity, *E*: binding energy).

Figure 2 shows the XRD pattern and TEM images of the n-Si prepared with dodecyltrimethylammonium bromide (DTAB) surfactant. This XRD pattern is identical to that of the n-Si prepared with OTAB, but the peaks are sharper. The estimated particle size of 10 nm agrees with the TEM image (Figure 2b). Thus, a longer alkyl chain length of the surfactant leads to a smaller particle size. Si nanoparticles 5 nm in size could not be obtained by using DTAB as surfactant, and 10 nm sized particles were the smallest we could prepare with DTAB. The high-resolution image shows

[*] H. Kim, M. Seo, M.-H. Park, Prof. J. Cho
School of Energy Engineering and Converging Research Center for Innovative Battery Technologies
Ulsan National Institute of Science & Technology
Ulsan, 689-798 (Korea)
E-mail: jpcho@unist.ac.kr
Homepage: http://jpcho.com

[**] This research was supported by the Converging Research Center Program through the National Research Foundation of Korea (NRF) funded by the Ministry of Education, Science and Technology.

Supporting information for this article is available on the WWW under http://dx.doi.org/10.1002/anie.200906287.

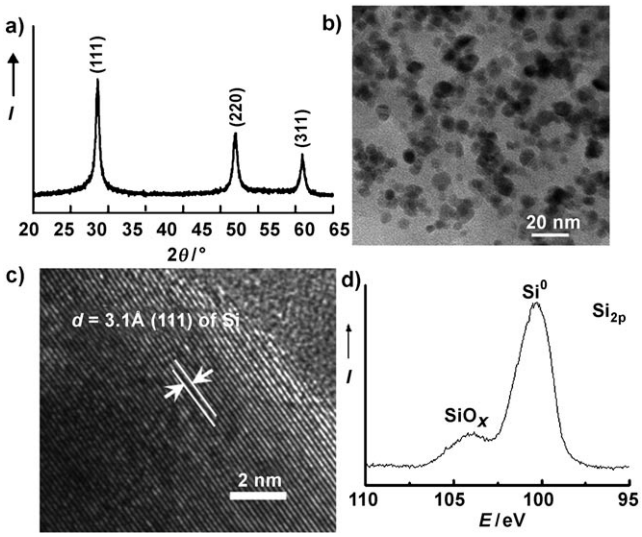

Figure 2. a) XRD pattern, b) and c) TEM images, and d) XPS spectrum of the 10 nm sized n-Si prepared with DTAB surfactant.

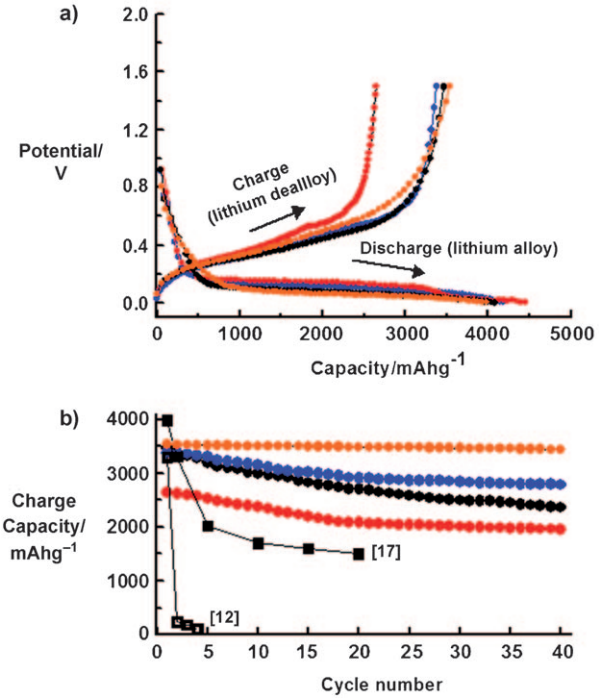

Figure 3. a) Voltage profiles of 5, 10, and 20 nm sized n-Si and 10 nm sized n-Si after carbon coating during the first cycle in coin-type half-cells at a rate of 0.2 C between 0 and 1.5 V. b) Plot of charge capacity versus cycle number (red: 5 nm, blue: 10 nm, orange: 10 nm after carbon coating, black circles: 20 nm).

the lattice fringe of the (111) plane, corresponding to a *d* spacing of 3.1 Å for the diamond cubic Si phase. The XP spectrum of the n-Si prepared with DTAB shows a much weaker peak for SiO_x at about 104 eV than the 5 nm sample. In general, Si containing larger amounts of SiO_x leads to larger irreversible capacity due to decomposition of SiO_x to Si and $x\,Li_2O$. Accordingly, higher Coulombic efficiency of n-Si prepared from DTAB than that from OTAB is expected. However, increasing the Si particle size to 20 nm was found to be impossible by using surfactant, and hence as-prepared 10 nm sized particles were annealed at 900 °C for 3 h to obtain 20 nm sized ones. Figure S1a (Supporting Information) shows a TEM image of 20 nm sized particles, which are well dispersed.

Figure 3a shows the discharge and charge curves during the first cycle in a coin-type half-cell between 0 and 1.5 V at a rate of 0.2 C (= 900 mA g^{-1}). The n-Si with an average particle size of 5 nm shows first discharge and charge capacities of 4443 and 2649 mAh g^{-1}, that is, a Coulombic efficiency of 60 %. On the other hand, the 10 nm sized particles, with capacities of 4210 and 3380 mAh g^{-1}, show a Coulombic efficiency of 80 %. In the case of 20 nm sized particles, discharge and charge capacities of 4080 and 3467 mAh g^{-1}, respectively, correspond to 85 % Coulombic efficiency. The decreased irreversible capacity of the particles with increasing size results from decreased formation of the nonconducting solid–electrolyte interface (SEI) due to the decreased surface area. Reduced SEI formation can lead to higher Coulombic efficiency in the 20 nm sized samples. Aurbach et al. reported that the irreversible capacity of the nanoparticles is closely related to the intensive side reactions between the active material and electrolyte species (especially $LiPF_6$).[16] This leads to generation of a nonconducting SEI layer. Furthermore, the surface area of the metal increases with decreasing particle size; thus, the amount of Li that is irreversibly consumed during the formation of SEI should also increase. These phenomena also contribute to capacity fading in the cell. In addition, decreased formation of SiO_x leads to improved Coulombic efficiency. As can be seen in Figure SI2 (Supporting Information), Coulombic efficiencies of the 5, 10, and 20 nm sized n-Si were 90, 93, and 92 %, respectively, while carbon-coated 10 nm sized n-Si showed 98 % efficiency up to 40 cycles.

Figure 3b compares the capacity retention of 5, 10, and 20 nm sized n-Si nanoparticles up to 40 cycles. They respectively show capacity retentions of 71, 81, and 67 %, after 40 cycles. Overall, 10 nm sized n-Si shows the highest capacity retention among the samples. This retention value is far superior to previous results. Ma et al. reported a first charge capacity of 4000 mAh g^{-1} for nestlike Si particles. The capacity retention after 20 cycles, however, was 38 %.[17] On the other hand, commercial Si powder consisting of strongly aggregated nanoparticles with an average particle size greater than 50 nm showed rapid capacity fade after only two cycles at 214 mAh g^{-1}.[12] Li et al. reported that Si nanoparticles obtained from SiH_4 decomposition showed a first charge capacity of 2000 mAh g^{-1}, which decreased to 150 mAh g^{-1} after 20 cycles.[18] Gao et al. reported that Si nanowires created by a laser ablation method exhibited a charge capacity of about 700 mAh g^{-1}.[19] These results indicate that nanostructured Si can become severely contaminated with SiO_x except for bulky hollow Si.[17] The significantly improved capacity retention of the present samples compared with those in other studies results from the uniformly distributed Si nanoparticles that were dispersed between the carbon black in the composite electrode. Hence, although Si nanoparticles

may be pulverized as a result of a large volume change, the electrical connection between them is maintained by the carbon black. Nonetheless, many studies in which silicon/carbon composites were used to improve the cycle life of Si reported that commercially available Si powder became severely aggregated with nanoparticles greater than 30 nm in size.[20–23] Therefore, it is impossible to coat carbon onto the Si nanoparticles uniformly.

When 10 nm sized Si particles were coated with carbon, a particle size similar to that of the pristine counterpart was observed, and the Raman spectrum of the sample confirmed formation of an amorphous carbon coating layer (Supporting Information SI3). The charge capacity (3535 mAh g^{-1}) and Coulombic efficiency for the first cycle (89%) are much improved over those of the pristine counterpart, and this confirms the role of the carbon layers in diminishing side reactions with the electrolytes. Furthermore, its capacity retention was 96% after 40 cycles. Sony researchers reported that a tin-based amorphous anode led to a 30% greater volumetric capacity than conventional graphite anode.[24] Later, Whittingham et al. confirmed that the Sn-based electrode consisted of an Sn–Co–Ti–graphite composite, the particle size of which was smaller than 300 nm.[25] Since the electrode density of the carbon-coated 10 nm sized n-Si anode was estimated to 1.3 g cm^{-3} after charging (lithium dealloying), the volumetric energy density of the cell was estimated to be 4596 mAh cm^{-3}. On the other hand, natural graphite was estimated to have 560 mAh cm^{-3} (electrode density and reversible capacity were 1.6 g cm^{-3} and 350 mAh g^{-1}). As a consequence, our n-Si anode has eight times higher volumetric energy density than graphite.

Figure 4 shows TEM images of the 5 and 10 nm sized n-Si nanoparticles after 40 cycles, and the 5 nm sized particles show no particle growth after cycling. Extracted n-Si particles from the composite electrode were aggregated and their images were very difficult to observe. In spite of this problem, our images provide clear evidence for estimating the particle size even after cycling. Previous studies on Si nanowires with a diameter of about 100 nm and nanotubes with a wall thickness of less than 100 nm clearly demonstrated increased wire diameter and wall thickness after cycling.[26–29] The 10 nm sized n-Si sample shows mixed amorphous and crystalline phases but appears to retain its pristine particle size after cycling (Figure 4b). At this time, although further fundamental work is necessary to elucidate this difference, this effect could be because the surface area to volume ratio increases dramatically when size decreases to the nanometer range, and any dislocations may be quickly drawn to the surface.[9,29] This agrees with the previous finding that fracture toughness of lithiated silicon nanoparticles smaller than 20 nm[30] or nanowires smaller than 100 nm is significantly improved.[30] The above results indicate that the critical Si particle size is 10 nm and that the particles should be coated with carbon to improve the cycle life and Coulombic efficiency. The 20 nm sized n-Si shows only an amorphous phase with loss of its original morphology (Supporting Information SI2b).

In conclusion, n-Si prepared at 380 °C and under high pressure shows different particle sizes depending on the surfactant. This is a new means of obtaining well-dispersed nanoparticles without aggregation. Although 10 nm sized Si particles showed the highest charge capacity, they exhibit lower Coulombic efficiency than 20 nm sized n-Si and a low capacity retention of 81%. When carbon coating was applied to 10 nm sized n-Si, however, both Coulombic efficiency and capacity retention were significantly improved, to 89 and 96%, respectively.

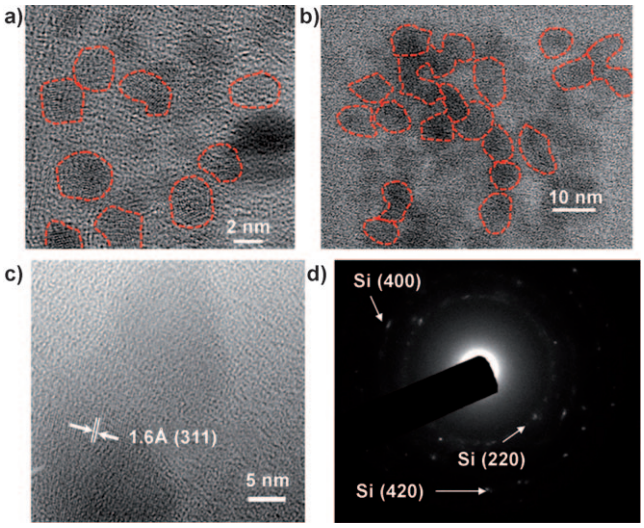

Figure 4. Ex situ TEM images of a) 5 nm sized Si particles (red lines indicate n-Si crystallites), b) and c) 10 nm sized particles (red lines indicate n-Si particles), and d) selected area diffraction pattern of (c) after 40 cycles (arrows indicate crystalline regions). All electrodes were dissembled after fully charging to 1.5 V (after lithium removal).

Experimental Section

Silicon nanoparticles were prepared in reverse micelles at high pressure and temperature in a bomb. OTAB or DTAB was used as surfactant for the following syntheses. All experiments were carried out in a glove box with <20 ppm oxygen. The synthesis was carried out in a 250 mL Hastelloy Parr reactor, equipped with a thermocontroller, a magnetic stirrer, and a cooling coil. In a typical synthesis, $SiCl_4$ (0.1 mol, anhydrous, 99.999%) was dissolved in a solution of OTAB or DTAB (1.5 g) in anhydrous THF (150 mL). This solution was then mixed with 25 mL of a previously prepared solution of naphthalene sodium (3 g) in THF, followed by pouring into the reactor vessel. The vessel was pumped down to about 150 mTorr and the temperature increased to 380 °C and maintained for 1 d. After cooling, the bomb was opened to the atmosphere and the product collected by filtration and washed several times with an excess of hexane and water to remove naphthalene and NaCl byproduct. The final product was annealed at 600 °C for 1 h to decompose residual surfactant under Ar stream in a tube furnace. Most of the anode particles differed in size less than 2 nm.

For carbon coating of 10 nm sized n-Si, acetylene gas was fed into a tube furnace in an Ar stream at 500 °C for 2 h. The carbon content of the product was about 6 wt%. The anodes for the battery test cells were made of n-Si, super P carbon black, and poly(vinylidene fluoride) (PVDF), binder (Solef) in a weight ratio of 80:10:10. The slurry was prepared by thoroughly mixing an solution of PVDF in *N*-methyl-2-pyrrolidone (NMP, Aldrich), carbon black, and the anode material. The coin-type half-cells (2016R size), prepared in a helium-filled glove box, contained n-Si, Li metal, a microporous polyethylene separator, and an electrolyte solution of 1M $LiPF_6$ in ethylene

carbonate/dimethyl carbonate (EC/DMC, 1:1 v/v; LG Chem., Korea). The loading of pure active material was 9 mg cm^{-2}, and therefore 0.2 C (= 900 mA g^{-1}) corresponded to 8.1 mA cm^{-2}. The same charge and discharge rates were used for cycling tests. For the ex situ TEM analysis of the cycled samples, the composite electrode was dissembled from the cell and dispersed in acetone with ultrasonic treatment.

A field-emission transition electron microscope (FE-TEM) (JEOL 2010F), operating at 200 KV, was used for investigating the microstructure of the samples. X-ray photoelectron spectroscopy (XPS) was performed on a Thermo Scientific K_α spectrometer with monochromatic $Al_{K\alpha}$ radiation (1486.6 eV). Spectra were recorded in the constant-pass energy mode at 50.0 eV. Raman measurements were performed with a Renishaw 2000 Raman microscope system. A Melles Griot He–Ne laser operating at $\lambda = 632.8$ nm was used as excitation source with a laser power of approximately 30 mW. The Rayleigh line was removed from the collected Raman scattering by using a holographic notch filter located in the collection path. Raman scattering was collected with a charge-coupled device (CCD) camera at a spectral resolution of 4 cm^{-1}. Each spectrum was accumulated three times with an exposure time of 30 s by using × 50 objective lens.

Received: November 8, 2009
Revised: December 27, 2009
Published online: February 19, 2010

Keywords: batteries · carbon · electrochemistry · lithium · silicon

[1] M. Winter, J. O. Besenhard, *Electrochim. Acta* **1999**, *45*, 31.
[2] J. Yang, M. Winter, J. P. Besenhard, *J. Power Sources* **1996**, *90*, 281.
[3] Y. Kwon, H. Kim, S. G. Doo, J. Cho, *Chem. Mater.* **2007**, *19*, 982.
[4] Y. Kwon, J. Cho, *Chem. Commun.* **2008**, 1109; M. G. Kim, J. Cho, *Adv. Funct. Mater.* **2009**, *19*, 1497; D. Deng, M. G. Kim, J. Y. Lee, J. Cho, *Energy Environ. Sci.* **2009**, *2*, 818.
[5] H. Takagi, H. Ogawa, Y. Yamazaki, A. Ishizaki, T. Nakagiri, *Appl. Phys. Lett.* **1990**, *56*, 2379.
[6] K. A. Littau, P. J. Szajowki, A. J. Muller, A. R. Kortan, L. E. Brus, *J. Phys. Chem.* **1993**, *97*, 1224.
[7] M. Holzapfel, H. Buqa, W. Scheifele, P. Novák, F. M. Petrat, *Chem. Commun.* **2005**, 1566.
[8] Y. Osaka, K. Tsunetomo, F. Toyomura, H. Myoren, K. Kohno, *Jpn. J. Appl. Phys. Part 2* **1992**, *31*, L365.
[9] J. Graetz, C. C. Ahn, R. Yazami, B. Fultz, *Electrochem. Solid-State Lett.* **2003**, *6*, A194.
[10] a) J. R. Heath, *Science* **1992**, *258*, 1131; P. E. Batson, J. R. Heath, *Phys. Rev. Lett.* **1993**, *71*, 911.
[11] R. K. Baldwin, K. A. Pettilgrew, E. Ratai, M. P. Augustine, S. M. Kauzlarich, *Chem. Commun.* **2002**, 1822.
[12] Y. Kwon, G. S. Park, J. Cho, *Electrochim. Acta* **2007**, *52*, 4663.
[13] J. H. Warner, A. Hoshino, K. Yamamoto, R. D. Tilley, *Angew. Chem.* **2005**, *117*, 4626; *Angew. Chem. Int. Ed.* **2005**, *44*, 4550.
[14] J. P. Wilcoxon, G. A. Samara, *Appl. Phys. Lett.* **1999**, *74*, 3164; J. P. Wilcoxon, G. A. Samara, P. N. Provencio, *Phys. Rev. B* **1999**, *60*, 2704.
[15] D. S. English, L. E. Pell, Z. Yu, P. F. Barbara, B. A. Krogel, *Nano Lett.* **2002**, *2*, 681.
[16] D. Aurbach, A. Nimberger, B. Markovsky, E. Levi, E. Sominski, A. Gedanken, *Chem. Mater.* **2002**, *14*, 4155.
[17] H. Ma, F. Cheng, J. Chen, J. Zhao, C. Li, Z. Tao, J. Liang, *Adv. Mater.* **2007**, *19*, 4067.
[18] H. Li, X. Haung, L. Chen, Z. Wu, Y. Liang, *Electrochem. Solid-State Lett.* **1999**, *2*, 547.
[19] B. Gao, S. Sinha, L. Fleming, O. Zhou, *Adv. Mater.* **2001**, *13*, 816.
[20] Y.-S. Hu, R. Demir-Caken, M. M. Titrici, J. O. Müller, R. Schlögl, M. Antonietti, J. Maier, *Angew. Chem.* **2008**, *120*, 1669 – 1673; *Angew. Chem. Int. Ed.* **2008**, *47*, 1645.
[21] G. X. Wang, J. Yao, H. K. Liu, *Electrochem. Solid-State Lett.* **2004**, *7*, A250.
[22] J. Yang, B. F. Wang, K. Wang, Y. Liu, J. Y. Xie, Z. S. Wen, *Electrochem. Solid-State Lett.* **2003**, *6*, A154.
[23] S. H. Ng, J. Z. Wang, D. Wexler, K. Konstantinov, Z. P. Guo, H. K. Liu, *Angew. Chem.* **2006**, *118*, 7050; *Angew. Chem. Int. Ed.* **2006**, *45*, 6896.
[24] http://www.sony.net/SonyInfo/News/Press/200502/05-006E.
[25] Q. Fan, P. J. Chupas, M. S. Whittingham, *Electrochem. Solid-State Lett.* **2007**, *20*, A217.
[26] M. H. Park, M. G. Kim, J. Joo, Y, Ciu, J. Cho, *Nano Lett.* **2009**, *9*, 3844.
[27] L. Y. Cui, Y. Cui, *Nano Lett.* **2009**, *9*, 191.
[28] H. Kim, J. Cho, *Nano Lett.* **2008**, *8*, 3688.
[29] H. Kim, B. Han, J. Choo, J. Cho, *Angew. Chem.* **2008**, *120*, 10305; *Angew. Chem. Int. Ed.* **2008**, *47*, 10151.
[30] M. H. Park, K. Kim, J. Kim, J. Cho, *Adv. Mater.* **2010**, *22*, 415.

